Asymptotic relationship between homoclinic points and periodic orbit stability exponents

Jizhou Li and Steven Tomsovic
Department of Physics and Astronomy, Washington State University, Pullman, Washington 99164-2814, USA

(Received 2 September 2019; published 4 November 2019)

The magnitudes of the terms in periodic orbit semiclassical trace formulas are determined by the orbits' stability exponents. In this paper, we demonstrate a simple asymptotic relationship between those stability exponents and the phase-space positions of particular homoclinic points.

DOI: 10.1103/PhysRevE.100.052202

I. INTRODUCTION

A variety of properties of chaotic quantum systems can be calculated with semiclassical trace formulas, which are sums over certain sets of classical orbits (periodic, heteroclinic, or closed orbits, etc.) arising in their classical counterparts. For example, Gutzwiller's trace formula [1] is a sum over periodic orbits that determines the spectrum, and the near-threshold absorption spectra of an atom in a magnetic field involve a sum over closed orbits that begin and end at the nucleus [2,3]. Such orbit sums properly account for quantum interferences as each orbit carries a magnitude determined by its stability exponent, and a phase factor determined by its classical action and Maslov index. The orbits with shorter periods give long-range structure to the quantum spectra, and the longer the period orbits are, the finer scale is the structure. Due to exponential proliferation and instability, explicit construction of a complete set of orbits with longer and longer periods rapidly becomes prohibitive.

In two previous publications [4,5], we developed an analytic scheme to express the classical actions of unstable periodic orbits in terms of action differences between certain homoclinic orbits. The homoclinic orbit action differences can then be obtained as phase-space integrals along the stable and unstable manifolds, which can be calculated stably by efficient numerical techniques [6–9]. Thus, the phase factors can be obtained via stable computations without the explicit construction of the orbits. Here, we address the magnitudes, i.e., the stability exponents of the periodic orbits. A new relationship is developed to link the stability exponents of unstable periodic orbits to the phase-space positions of specific homoclinic points. The exponent is determined by the ratio between relative positions from an asymptotic family of homoclinic points. Thus, the periodic orbit magnitudes can also be determined without explicit construction. This implies a unified scheme of interchanging the periodic orbits with homoclinic orbits, which may be very beneficial depending on the circumstances.

The paper is organized as follows: Section II introduces the basic concepts of hyperbolic orbits and the main language for the description of unstable orbits— symbolic dynamics. A generic model for the symbolic dynamics, the Smale horseshoe [10,11], is also introduced in this section. Section III is the main content of this work, which develops the central theorem. Section IV provides numerical verification. Section V makes a brief conclusion and points to directions for future work.

II. BASIC CONCEPTS

A. Symbolic dynamics

Let us consider a two-degree-of-freedom chaotic Hamiltonian system. With energy conservation and applying the Poincaré surface of section technique [12], the Hamiltonian flow is reduced to a discrete area-preserving map M on the two-dimensional phase space (q, p). Assuming the dynamics of the Hamiltonian systems is hyperbolic, the corresponding Poincaré map M is also hyperbolic. The orbit of a phase-space point z_0, denoted by $\{z_0\}$, is the bi-infinite collection of all $M^n(z_0)$:

$$\begin{aligned}\{z_0\} &= \{\dots, M^{-1}(z_0), z_0, M(z_0), \dots\} \\ &= \{\dots, z_{-1}, z_0, z_1, \dots\},\end{aligned}$$

where $z_n = M^n(z_0)$ for all n. Generic orbits are hyperbolic, or exponentially unstable, as two orbits starting from nearby initial conditions will typically be separated exponentially under successive iterations. The exponential rate of a typical orbit is captured by the Lyapunov exponent, μ, which quantifies the mean stretching and compressing rate of the hyperbolic map. In open systems, such stretching and compressing behaviors of the dynamics lead to certain *escaping orbits* that tend to infinity under successive inverse or forward iterations. However, we concentrate on the orbits that do not escape to infinity, the *nonwandering set* (the results apply equally well in closed systems). Denote the set of interest by Ω. The main object of study in this article, namely the homoclinic and periodic orbits, all belong to Ω.

Let $x = (q, p)$ be a hyperbolic fixed point from Ω, i.e., $M(x) = x$. Denote the unstable and stable manifolds of x by $U(x)$ and $S(x)$, respectively. Typically, $U(x)$ and $S(x)$ intersect infinitely many times and form a complicated pattern called a homoclinic tangle [12–14]. The notation $U[a, b]$ is introduced to denote the finite segment of $U(x)$ extending from a to b, both of which are points on $U(x)$, and similarly for $S(x)$. These manifolds are important skeleton-like structures of the dynamics since the exponential stretching and compressing

of the map are fully captured by the unstable and stable manifolds, respectively. Furthermore, the folding of phase-space regions is also described by the folding of the manifolds.

It is well known that Markov partitions to the phase space [15,16] exist that use segments on $U(x)$ and $S(x)$ as boundaries, which are used to assign symbolic dynamics [17–20] as phase-space itineraries of orbits in Ω. The cells of the partition $\mathcal{V} = [V_0, V_1, \ldots, V_L]$ are closed curvilinear parallelograms bounded by the stable and unstable manifolds. The symbolic dynamics assigns a one-to-one correspondence between orbits of the system and sequences of symbols taken from an alphabet, $s_i \in [0, 1, \ldots, L]$, which are in one-to-one correspondence with the cells $[V_0, V_1, \ldots, V_L]$ [16]. The symbolic code of a phase-space point z_0 is then a bi-infinite sequence of alphabets,

$$z_0 \Rightarrow \cdots s_{-2}s_{-1} \cdot s_0 s_1 s_2 \cdots , \tag{1}$$

where each digit s_n in the symbol denotes the cell in which $M^n(z_0)$ belongs to $M^n(z_0) = z_n \in V_{s_n}$, $s_n \in \{0, \ldots, L\}$. The dot in the middle indicates the current iteration: $z_0 \in V_{s_0}$. In that sense, the symbolic code gives an "itinerary" of z_0 under successive forward and backward iterations, in terms of the Markov cells in which each iteration lies. The mapping M under the symbolic dynamics is then reduced to a simple shift of the dot in the code:

$$M^n(z_0) = z_n \Rightarrow \cdots s_{n-1} \cdot s_n s_{n+1} \cdots .$$

Points along the same orbit have the same symbolic strings but shifting dots. Therefore, an orbit can be represented by the symbolic string without the dot.

B. The horseshoe map

Assuming the system is highly chaotic, the homoclinic tangle forms a complete horseshoe, part of which is shown in Fig. 1, as this is generic to a significant class of dynamical systems. In such scenarios, the Markov partition is a simple set of two regions $[V_0, V_1]$, as shown in the upper panel of Fig. 1. Each phase-space point z_0 that never escapes to infinity can be put into a one-to-one correspondence with a bi-infinite symbolic string in Eq. (1), where each digit $s_n \in 0, 1$ such that $M^n(z_0) \in V_{s_n}$.

Throughout this paper, we use the area-preserving Hénon map [21] with parameter $a = 10$ for illustration and numerical implementations:

$$\begin{aligned} p_{n+1} &= q_n, \\ q_{n+1} &= a - q_n^2 - p_n. \end{aligned} \tag{2}$$

This parameter is well beyond the first tangency, thus giving rise to a complete horseshoe-shaped homoclinic tangle with highly chaotic dynamics. It serves as a simple paradigm since the symbolic dynamics permits all possible combinations of binary codes, and no "pruning" [22,23] is needed. The results derived below mostly carry over into more complicated systems possessing incomplete horseshoes, or systems with more than binary symbolic codes, though more work is needed to address such systems. Appendix A of [5] has more details on the partition and symbolic dynamics relevant here.

The intersections between $S(x)$ and $U(x)$ give rise to homoclinic orbits, which are asymptotic to x under both $M^{\pm\infty}$.

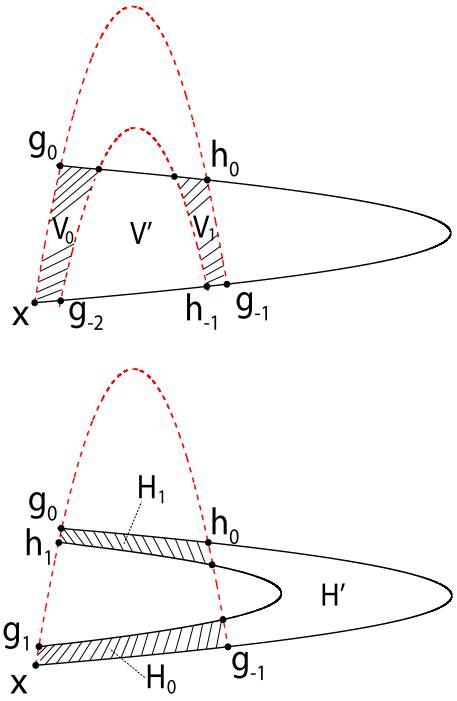

FIG. 1. Example partial homoclinic tangle from the Hénon map, which forms a complete horseshoe structure. The unstable (stable) manifold of x is the solid (dashed) curve. There are two primary homoclinic orbits: $\{h_0\}$ and $\{g_0\}$. Let $\mathcal{R}$ be the closed region bounded by manifold segments $U[x, g_{-1}]$, $S[g_{-1}, h_0]$, $U[h_0, g_0]$, and $S[g_0, x]$. In the upper panel, $\mathcal{R}$ can be identified as the region composed by V_0, V', and V_1. Under forward iteration, the vertical strips V_0 and V_1 (including the boundaries) from the upper panel are mapped into the horizontal strips H_0 and H_1 in the lower panel. At the same time, points in region V' are mapped outside $\mathcal{R}$ into region H', never to return and escape to infinity. There is a Cantor set of points in V_0 and V_1 that remain inside $\mathcal{R}$ for all iterations, which is the nonwandering set Ω. The phase-space itineraries of points in Ω in terms of V_0 and V_1 give rise to symbolic dynamics.

From the infinite families of homoclinic orbits, two special ones, $\{h_0\}$ and $\{g_0\}$, can be identified as primary homoclinic orbits in the sense that they have the simplest phase-space excursions. The segments $S[x, h_0]$ and $U[x, h_0]$ intersect only at h_0 and x, and the same is true for all its orbit points h_i; this holds for $\{g_0\}$ as well. There are only two primary orbits for the horseshoe, but possibly more for systems with more complicated homoclinic tangles.

Under the symbolic dynamics, a period-T point y_0, where $M^T(y_0) = y_0$, can always be associated with a symbolic string with infinite repetitions of a substring with length T:

$$y_0 \Rightarrow \cdots s_0 s_1 \cdots s_{T-1} \cdot s_0 s_1 \cdots s_{T-1} \cdots = \overline{\gamma} \cdot \overline{\gamma}, \tag{3}$$

where $\gamma = s_0 \cdots s_{T-1}$ is the finite substring, and $\overline{\gamma} \cdot \overline{\gamma}$ denotes its infinite repetition (on both sides of the dot). Notice that the cyclic permutations of $s_0 \cdots s_{T-1}$ can be associated with the successive mappings of y_0, generating a one-to-one mapping to the set of points on the orbit. Since an orbit can be represented by any point on it, the position of the dot does not matter, therefore we denote the periodic orbit $\{y_0\}$ as

$$\{y_0\} \Rightarrow \overline{\gamma} \tag{4}$$

with the dot removed. Similarly, the finite length-T orbit segment $[y_0, y_1, \ldots, y_{T-1}]$, which composes one full period, is denoted

$$y_0, y_1, \ldots, y_{T-1} \Rightarrow \gamma \tag{5}$$

with the overhead bar removed, as compared to Eq. (4). Any cyclic permutation of γ refers to the same periodic orbit.

The hyperbolic fixed point has the simplest symbolic code $x \Rightarrow \overline{0} \cdot \overline{0}$, and its orbit $\{x\} \Rightarrow \overline{0}$ correspondingly. A homoclinic point h_0 of x has a symbolic code of the form [24]

$$h_0 \Rightarrow \overline{0}1 s_{-m} \cdots s_{-1} \cdot s_0 s_1 \cdots s_n 1\overline{0} \tag{6}$$

along with all possible shifts of the dot, where the $\overline{0}$ on both ends means the orbit approaches the fixed point (therefore it stays in V_0) under both $M^{\pm\infty}$. Similar to the periodic orbit case, the homoclinic orbit can be represented as

$$\{h_0\} \Rightarrow \overline{0}1 s_{-m} \cdots s_{-1} s_0 s_1 \cdots s_n 1\overline{0} \tag{7}$$

with the dot removed, as compared to Eq. (6).

A *heteroclinic* orbit $\{h_0'\}$ between the periodic point $y \Rightarrow \overline{\gamma} \cdot \overline{\gamma}$ and the fixed-point $x \Rightarrow \overline{0} \cdot \overline{0}$ arises from $h_0' = U(y) \cap S(x)$, and it can be represented by

$$\{h_0'\} \Rightarrow \overline{\gamma} \gamma' \overline{0}, \tag{8}$$

where the asymptotic behaviors of the orbit are described by $\overline{\gamma}$ and $\overline{0}$ on the two ends, and the finite symbolic string γ' describes the connection from $\{y\}$ to $\{x\}$, which depends solely on the choice of h_0'.

III. PERIODIC ORBIT STABILITY EXPONENT

Consider an arbitrary unstable periodic orbit $\{y\}$ with symbolic code $\{y\} \Rightarrow \overline{\gamma}$. Let the length of the symbolic string γ be n_γ, which is also the periodic of $\{y\}$. The periodic point y can also be viewed as a fixed-point under the n_γth compound mapping of M: $M^{n_\gamma}(y) = y$. Denote the eigenvalue of the unstable subspace of the tangent space of $\{y\}$ under one full period (n_γ) by λ_γ. Thus $\lambda_\gamma > 1$ if $\{y\}$ is hyperbolic without reflection ($\lambda_\gamma < -1$ with reflection). The stability exponent of $\{y\}$, denoted by μ_γ, is then $n_\gamma \mu_\gamma = \ln |\lambda_\gamma|$.

To help determine λ_γ and thus μ_γ, choose a family of auxiliary homoclinic points of the fixed-point x, namely $h_0^{(m)}$ ($m = 1, 2, \ldots$), that has the symbolic codes

$$h_0^{(m)} \Rightarrow \overline{0} \gamma^m \cdot \overline{0}, \tag{9}$$

where γ^m denotes m repetitions of γ and $m = 1, 2, \ldots$. Having identified the auxiliary homoclinic points, let us consider the homoclinic orbit segments generated by certain numbers of inverse iterations of them, namely

$$\text{Seg(k,m)} = \left\{h_{-N(k,m)}^{(m)}, \ldots, h_{-1}^{(m)}, h_0^{(m)}\right\}, \tag{10}$$

where $N(k, m) = (k + m)n_\gamma$ is a positive integer determined by k and m ($k, m \geqslant 1$). Ahead k is taken to ∞, which yields the limit

$$\lim_{k\to\infty} h_{-N(k,m)}^{(m)} = x. \tag{11}$$

The key to the derivation lies in the *normal-form* transformation [25–27] of three orbit segments. For well-behaved

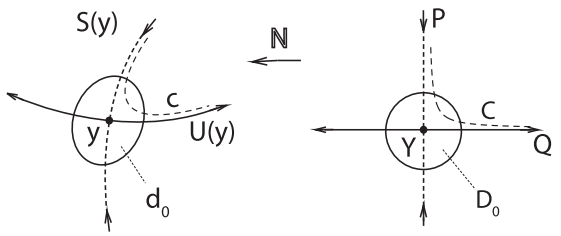

FIG. 2. Schematic visualization of the normal form transformation $\mathbb{N}$. It transforms points from the normal form coordinate (Q, P) into the phase-space coordinate (q, p). The Q and P axes are mapped into $U(y)$ and $S(y)$, respectively. The advantage of normal form coordinates is that the dynamics preserves the QP product [Eq. (12)], thus points are mapped along invariant hyperbolas, as shown by C in the right panel. The family of invariant hyperbolas then gives rise to a family of Moser invariant curves in phase space via the transformation $\mathbb{N}(C) = c$, shown in the left panel.

(invertible and analytic) Poincaré maps, the nonlinear dynamics near the stable and unstable manifolds can be linearized via a common technique called *normal-form transformation*, denoted by $\mathbb{N}$, which transforms points from the normal form coordinates (Q, P) to the neighborhood of stable and unstable manifolds of the hyperbolic fixed point y: $\mathbb{N} : (Q, P) \mapsto (q, p)$, as shown in Fig. 2. In the normal-form coordinates of y, the compound mapping M^{n_γ} takes a simple form:

$$\begin{aligned} Q_{n+1} &= \Lambda(Q_n P_n) Q_n, \\ P_{n+1} &= [\Lambda(Q_n P_n)]^{-1} P_n, \end{aligned} \tag{12}$$

where $\Lambda(Q_n P_n)$ is a polynomial function of the product $Q_n P_n$ [28]:

$$\Lambda(QP) = \lambda_\gamma + w_2(QP) + w_3(QP)^2 + \cdots. \tag{13}$$

The normal form convergence zone was first proved by Moser [26] to be a small disk-shaped region centered at the fixed point (D_0 and its image d_0 in Fig. 2), and later proved by da Silva Ritter *et al.* [27] to extend along the stable and unstable manifolds to infinity. The extended convergence zone follows hyperbolas to the manifolds ("gets exponentially close" the further out along the manifolds). The stable and unstable manifolds are just images of the P and Q axes, respectively, under the normal form transformation.

All points inside the extended convergence zone near the Q or P axis move along invariant hyperbolas, which are mapped to Moser invariant curves in phase space. A schematic example is shown in Fig. 2, where the hyperbola C in the normal form coordinates is transformed into a Moser curve c in phase space. Being confined in the extended convergence zone, the Moser invariant curves also get exponentially close to the stable and unstable manifolds while extending along them outward to infinity. In fact, as shown by [28], the convergence zone can be quantified using the outermost Moser curve with the largest QP product.

Let the image of $\text{Seg}(k, m)$ in the normal-form coordinate of y be

$$\text{Seg(k,m)} = \left\{H_{-N(k,m)}^{(m)}, \ldots, H_{-1}^{(m)}, H_0^{(m)}\right\}, \tag{14}$$

where $\mathbb{N}(H_n^{(m)}) = h_n^{(m)}$. In the normal-form coordinates, every $\text{Seg}(k, m)$ lies on a hyperbola, labeled by C_m in Fig. 3. This

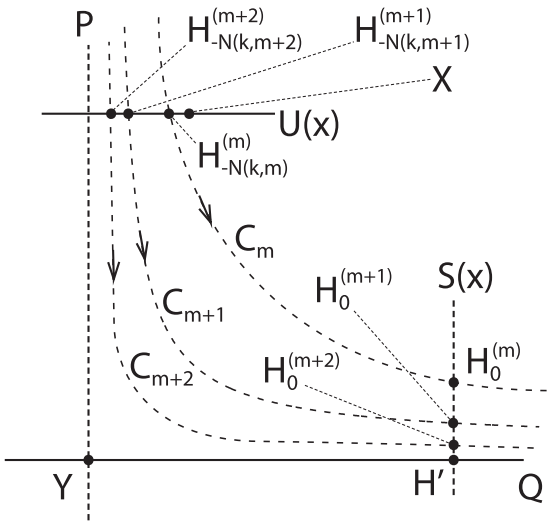

FIG. 3. (Schematic) Normal-form coordinate picture of the auxiliary homoclinic orbit segments. Y is the image of y, and the P and Q axes are the images of $S(y)$ and $U(y)$, respectively, in the normal-form coordinate. X is the image of the fixed-point x. Three auxiliary homoclinic orbit segments, corresponding to m, $m+1$, and $m+2$ in Eq. (14), lie on the hyperbolas C_m, C_{m+1}, and C_{m+2}, respectively. Note that only the first and the last points of each orbit segment are drawn here.

figure shows $\mathrm{Seg}(k,m)$, $\mathrm{Seg}(k,m+1)$, and $\mathrm{Seg}(k,m+2)$ in the normal-form coordinate of the periodic point y. Letting $k\to\infty$, because of Eq. (11), the initial points of the three segments, namely $H^{(m)}_{-N(k,m)}$, $H^{(m+1)}_{-N(k,m+1)}$, and $H^{(m+2)}_{-N(k,m+2)}$, are all located infinitesimally close to X along $U(x)$:

$$\lim_{k\to\infty} H^{(m)}_{-N(k,m)} = \lim_{k\to\infty} H^{(m+1)}_{-N(k,m+1)} = \lim_{k\to\infty} H^{(m+2)}_{-N(k,m+2)} = X. \tag{15}$$

Then, under $N(k,m)$, $N(k,m+1)$, and $N(k,m+2)$ iterations, respectively, they are mapped to the final points $H^{(m)}_0$, $H^{(m+1)}_0$, and $H^{(m+2)}_0$, as shown near the heteroclinic point H' on the Q axis. This heteroclinic point has the symbolic code

$$\mathbb{N}(H') = h' \Rightarrow \overline{\gamma}\cdot\overline{0}, \tag{16}$$

which is the simplest heteroclinic connection between $\{y\}$ and $\{x\}$. Recall that

$$\mathbb{N}\big(H^{(m)}_0\big) = h^{(m)}_0 \Rightarrow \overline{0}\gamma^m\cdot\overline{0}. \tag{17}$$

Comparing the symbolic strings in Eqs. (16) and (17), it follows that the codes of h' and $h^{(m)}_0$ to the right of the dot are identical, and to the left of the dot they match up to γ^m (which has length mn_γ). This indicates that $h^{(m)}_0$ is $\sim O(e^{-mn_\gamma\mu_\gamma})$ close to h' along $S(x)$ (for more details, see Appendix A of Ref. [5]). Due to the same reason, $h^{(m+1)}_0$ and $h^{(m+2)}_0$ are $\sim O(e^{-(m+1)n_\gamma\mu_\gamma})$ and $\sim O(e^{-(m+2)n_\gamma\mu_\gamma})$ close to h', respectively, along $S(x)$. Therefore, the three homoclinic points, $h^{(m)}_0$, $h^{(m+1)}_0$, and $h^{(m+2)}_0$, are all within an $\sim O(e^{-mn_\gamma\mu_\gamma})$ neighborhood of h'. See Fig. 3 for a schematic demonstration of this in the normal-form coordinate.

The same conclusion holds true in the normal-form coordinates. In fact, as shown by Fig. 3, in the normal coordinate of y, the proportionality factors of the distances between them can be determined analytically. Plotted in the figure are the initial and final points of $\mathrm{Seg}(k,m)$, $\mathrm{Seg}(k,m+1)$, and $\mathrm{Seg}(k,m+2)$. The k here is assumed to be a large integer, so $H^{(m)}_{-N(k,m)}$, $H^{(m+1)}_{-N(k,m+1)}$, and $H^{(m+2)}_{-N(k,m+2)}$ are exponentially close to X. Under successive forward iterations, they are mapped along the hyperbolas C_m, C_{m+1}, and C_{m+2}, respectively, into $H^{(m)}_0$, $H^{(m+1)}_0$, and $H^{(m+2)}_0$:

$$M^{N(k,m+i)}\big(H^{(m+i)}_{-N(k,m+i)}\big) = H^{(m+i)}_0, \tag{18}$$

where $i=0,1,2$. The mapping equations take the simple form of Eq. (12), with the stability factor Λ given by

$$\Lambda(QP) = \lambda_\gamma + w_2(QP) + w_3(QP)^2 + \cdots. \tag{19}$$

Under the limit $m\to\infty$, $H^{(m+i)}_0 \to H'$ $(i=0,1,2)$, so their QP products along the hyperbolas $\to 0$. Correspondingly, the stability factor $\Lambda(QP)\to\lambda_\gamma$, and the C_m curve becomes infinitely close to the P and Q axes when $m\to\infty$.

Consequently, the P coordinate values of $H^{(m+i)}_0$, namely $P(H^{(m+i)}_0)$, are determined asymptotically by

$$\lim_{m\to\infty} P\big(H^{(m+i)}_0\big) = \lim_{\substack{k\to\infty\\ m\to\infty}} P(X)\lambda_\gamma^{-(k+m+i)} \tag{20}$$

for $i=0,1,2,\ldots$, where $P(X)$ denotes the P-coordinate value of X. Furthermore, notice that $N(k,m+j)-N(k,m)=jn_\gamma$, thus using Eq. (20) we get

$$\lim_{m\to\infty} P\big(H^{(m+j)}_0\big) = \lim_{m\to\infty} P\big(H^{(m)}_0\big)\lambda_\gamma^{-j} \tag{21}$$

for $j=0,1,2,\ldots$. Therefore, the family of homoclinic points, $H^{(m+j)}_0$ $(j=0,1,2,\ldots)$, converges to H' under convergence factor λ_γ^{-1}. Since the normal-form transformation preserves the convergence factor of asymptotic series of points (see Appendix B 2 of Ref. [29] for a detailed proof), the family $h^{(m+j)}_0$ $(j=0,1,2,\ldots)$ also converges to h' in phase space. Therefore, their phase-space positions satisfy

$$\lim_{m\to\infty}\frac{p\big(h^{(m)}_0\big)-p(h')}{p\big(h^{(m+j)}_0\big)-p(h')} = \lambda_\gamma^j,$$
$$\lim_{m\to\infty}\frac{q\big(h^{(m)}_0\big)-q(h')}{q\big(h^{(m+j)}_0\big)-q(h')} = \lambda_\gamma^j, \tag{22}$$

where $p(a)$ and $q(a)$ denote the p- and q-coordinate values, respectively, of the point a. Here we assume the generic case that the local direction of $S(x)$ at h' is not strictly vertical or horizontal, so the differences between the p and q values of successive members do not vanish. The distances between successive members of the family are also in scale:

$$\lim_{m\to\infty}\frac{p\big(h^{(m)}_0\big)-p\big(h^{(m+1)}_0\big)}{p\big(h^{(m+1)}_0\big)-p\big(h^{(m+2)}_0\big)} = \lambda_\gamma, \tag{23}$$

and the same is true for the q coordinate values as well. Therefore, the stability exponent $n_\gamma\mu_\gamma = \ln|\lambda_\gamma|$ of the periodic orbit $\{y\}\Rightarrow\overline{\gamma}$ can be determined using Eq. (23) from the family of auxiliary homoclinic points $h^{(m)}_0\Rightarrow\overline{0}\gamma^m\cdot\overline{0}$, which does not require the numerical construction of the periodic orbit. In practice, for long periodic orbits with large periods

TABLE I. Unstable eigenvalues and the corresponding exponents of the periodic orbits in Eq. (25). λ_γ are calculated from the numerical orbits, and λ'_γ are determined from Eq. (24). The exponents are obtained as $n_\gamma \mu_\gamma = \ln|\lambda_\gamma|$ and $n_\gamma \mu'_\gamma = \ln|\lambda'_\gamma|$.

$\overline{\gamma}$	λ_γ	λ'_γ	$n_\gamma \mu_\gamma$	$n_\gamma \mu'_\gamma$
$\overline{1011}$	−586.069	−584.741	6.37343	6.37116
$\overline{0011}$	1602.00	1602.20	7.37900	7.37913
$\overline{0001}$	−2609.92	−2609.72	7.86707	7.86699
$\overline{00011}$	14176.1	14180.5	9.55931	9.55962

(n_γ), the leading terms in the $h_0^{(m)}$ family should provide an accurate enough calculation of λ_γ:

$$\lambda_\gamma \approx \frac{p\left(h_0^{(1)}\right) - p\left(h_0^{(2)}\right)}{p\left(h_0^{(2)}\right) - p\left(h_0^{(3)}\right)}. \tag{24}$$

IV. EXPLICIT EXAMPLE

To verify Eq. (24), we have numerically constructed four different periodic orbits in the Hénon map [Eq. (2)], namely $\{v\}$, $\{y\}$, $\{w\}$, and $\{z\}$, with symbolic codes

$$\begin{aligned} \{v\} &\Rightarrow \overline{1011}, \\ \{y\} &\Rightarrow \overline{0011}, \\ \{w\} &\Rightarrow \overline{0001}, \\ \{z\} &\Rightarrow \overline{00011}. \end{aligned} \tag{25}$$

The phase-space positions of one of their orbit points are

$$\begin{aligned} v &= (3.162\,277\,660\,168,\ 1.917\,144\,929\,227), \\ y &= (-3.162\,277\,660\,168,\ 3.162\,277\,660\,168), \\ w &= (-4.040\,365\,740\,912,\ -3.162\,277\,660\,168), \\ z &= (-3.300\,504\,906\,006,\ 3.181\,101\,045\,340), \end{aligned} \tag{26}$$

which are mapped back into themselves under their respective periods. Using these numerical orbits, their respective stability eigenvalues λ_γ and exponents μ_γ have been calculated. In addition, by constructing the respective auxiliary homoclinic points in Eq. (9) for each orbit, the same stability eigenvalues λ'_γ and exponents μ'_γ have been approximated with Eq. (24). The results are listed in Table I. Although only the leading terms in each auxiliary homoclinic family are used, due to the relatively long periods chosen in the examples ($n_\gamma \geqslant 4$), the resulting $n_\gamma \mu_\gamma$ products are all large enough to provide rapid convergence. Therefore, the agreement is excellent.

V. CONCLUSIONS

An exact formula [Eq. (23)] is introduced that links the stability properties of unstable periodic orbits to the phase-space locations of certain homoclinic points. Although the formula is asymptotic in nature, the numerical results from using the leading term already reproduce the actual exponents quite accurately in the numerical model used. Since the numerical computation of long periodic orbits suffers from an exponential instability problem, whereas the positions of homoclinic points can be determined relatively easily as the intersections between the invariant manifolds [6], this approach may provide an efficient alternative to direct calculations. Furthermore, in previous work [4,5], the classical actions of periodic orbits are expressed in terms of certain homoclinic orbit action differences. Combined with the current results, they provide a unified scheme of replacing the periodic orbits in the trace formula by homoclinic orbits, which may lead to new resummation techniques in semiclassical methods.

An important generalization of the current theory would be to extend it to higher-dimensional symplectic maps with chaotic dynamics. For instance, in four-dimensional (4D) maps, the stable and unstable manifolds of hyperbolic fixed points will each be two-dimensional surfaces. They intersect in the 4D phase-space generating homoclinic points. It may be the case that the relative positions of certain homoclinic points distributed along the dominant contraction direction in the stable manifolds yield the dominant stability exponent, and the relative positions of the homoclinic points along the subdominant contraction direction of the stable manifolds yield the subdominant stability exponent. However, the generalization of the symbolic code description to higher dimensions is a challenging issue.

[1] M. C. Gutzwiller, J. Math. Phys. **12**, 343 (1971), and references therein .

[2] M. L. Du and J. B. Delos, Phys. Rev. A **38**, 1896 (1988).

[3] M. L. Du and J. B. Delos, Phys. Rev. A **38**, 1913 (1988).

[4] J. Li and S. Tomsovic, Phys. Rev. E **95**, 062224 (2017).

[5] J. Li and S. Tomsovic, Phys. Rev. E **97**, 022216 (2018).

[6] J. Li and S. Tomsovic, J. Phys. A **50**, 135101 (2017).

[7] B. Krauskopf and H. M. Osinga, J. Comput. Phys. **146**, 404 (1998).

[8] A. M. Mancho, D. Small, S. Wiggins, and K. Ide, Physica D **182**, 188 (2003).

[9] B. Krauskopf, H. M. Osinga, E. J. Doedel, M. E. Henderson, J. Guckenheimer, A. Vladimirsky, M. Dellnitz, and O. Junge, Int. J. Bifurcation Chaos **15**, 763 (2005).

[10] S. Smale in *Differential and Combinatorial Topology*, edited by S. S. Cairns (Princeton University Press, Princeton, NJ, 1963).

[11] S. Smale, *The Mathematics of Time: Essays on Dynamical Systems, Economic Processes and Related Topics* (Springer-Verlag, New York, 1980).

[12] H. Poincaré, *Les Méthodes Nouvelles de la Mécanique Céleste* (Gauthier-Villars et Fils, Paris, 1899), Vol. 3 .

[13] R. W. Easton, Trans. Am. Math. Soc. **294**, 719 (1986).

[14] V. Rom-Kedar, Physica D **43**, 229 (1990).

[15] R. Bowen, *Lecture Notes in Mathematics Vol. 470* (Springer-Verlag, Berlin, 1975).

[16] P. Gaspard, *Chaos, Scattering and Statistical Mechanics* (Cambridge University Press, Cambridge, UK, 1998).

[17] J. Hadamard, J. Math. Pures Appl. series **54**, 27 (1898).

[18] G. D. Birkhoff, *AMS Coll. Publications* (American Mathematical Society, Providence, RI, 1927), Vol. 9.
[19] G. D. Birkhoff, Mem. Pont. Acad. Sci. Novi Lyncaei **1**, 85 (1935).
[20] M. Morse and G. A. Hedlund, Am. J. Math. **60**, 815 (1938).
[21] M. Hénon, Commun. Math. Phys. **50**, 69 (1976).
[22] P. Cvitanović, G. H. Gunaratne, and I. Procaccia, Phys. Rev. A **38**, 1503 (1988).
[23] P. Cvitanović, Physica D **51**, 138 (1991).
[24] R. Hagiwara and A. Shudo, J. Phys. A **37**, 10521 (2004).
[25] G. D. Birkhoff, Acta Math. **50**, 359 (1927).
[26] J. Moser, Commun. Pure Appl. Math. **9**, 673 (1956).
[27] G. L. da Silva Ritter, A. M. Ozorio de Almeida, and R. Douady, Physica D **29**, 181 (1987).
[28] M. Harsoula, G. Contopoulos, and C. Efthymiopoulos, J. Phys. A **48**, 135102 (2015).
[29] K. A. Mitchell, J. P. Handley, B. Tighe, J. B. Delos, and S. K. Knudson, Chaos **13**, 880 (2003).